TÜBİTAK

Turkish Journal of Chemistry

http://journals.tubitak.gov.tr/chem/

Research Article

Turk J Chem
(2021) 45: 1133-1145
© TÜBİTAK
doi:10.3906/kim-2010-67

Preparation of ethyl levulinate from wheat stalk over $Zr(SO_4)_2/SiO_2$

Ding-kai WANG, Wei ZHAO*, Ming-yu CUI, Tian-tian GUO, Shui-yuan FU, Wei-gang LI
Key Laboratory of Coal Processing and Efficient Utilization, China University of Mining & Technology, Jiangsu, China

Received: 31.10.2020 • **Accepted/Published Online:** 30.04.2021 • **Final Version:** 27.08.2021

Abstract: A series of $Zr(SO_4)_2/SiO_2$ solid acid catalysts with different $Zr(SO_4)_2$ loadings were prepared by water-soluble-impregnation method at room temperature. Then, the prepared catalysts were characterized by Fourier transform infrared spectroscopy, transmission electron microscopy and energy-dispersive X-ray spectrum, X-ray diffraction, adsorption/desorption of N_2, and temperature-programmed desorption of NH_3. The results showed that the active component $Zr(SO_4)_2$ was successfully adhered to the mesoporous SiO_2, and the acid amount of $Zr(SO_4)_2/SiO_2$ increased with the increasing of the $Zr(SO_4)_2$ loadings. Finally, the wheat stalk was used as raw material and depolymerized over $Zr(SO_4)_2/SiO_2$ to produce ethyl levulinate (EL). The reaction mixture was separated and purified by filtration and vacuum distillation. The kinetic characteristics and the reaction pathway were also studied. A comparative study showed that 20 wt.% $Zr(SO_4)_2/SiO_2$ exhibited higher catalytic activity. When reaction temperature, time, catalyst dosage and $Zr(SO_4)_2$ loadings were 190 °C, 50 min, 20 wt.% and 30 wt.%, the EL yield reached a maximum of 17.14%. The relative content of EL exceeded 90% after three steps of distillation.

Key words: Ethyl levulinate, glucose, solid acid $Zr(SO_4)_2/SiO_2$, wheat stalk

1. Introduction

With the development of economy, fossil resources, such as coal, oil and natural gas, are almost exhausted, and serious environmental problems have been caused. It is extremely urgent to make full use of green and renewable resources [1–3]. Biomass resource is the only renewable carbon source that can be used as the raw material for the productions of carbon-based chemicals and energy [4]. As an important biomass, crop straw with its great abundance and high utilization potential has attracted more and more attention [5–9]. The use of crop straw as a raw material for the production of value-added chemicals can obtain great economic benefit. As a kind of crop straw, wheat stalk is mainly composed of cellulose, hemicellulose, and lignin. Among them, cellulose, which accounts for 45% of wheat straw, is the main substrate for catalytic conversion to biofuel [10–12]. In previous studies on the preparation of valuable platform compounds, a relatively simple and effective way is the catalytic conversion of biomass-derived sugars to ethyl levulinate (EL) using various catalysts [13]. However, less attention has been paid to the conversion of crop straw to EL using an efficient catalyst. Based on current research status of crop straw utilization, it is important to increase the yield of valuable chemicals from direct conversion of crop straw [14–16].

As a chemical product with wide industrial application prospect, EL has been used in the fields of petroleum additives, perfume and pharmaceutical intermediates [17,18]. In addition, EL, being one of the levulinate esters (LE), contains ~14 mol% oxygen and has similar properties with fatty acid ethyl esters in biodiesel [19]. EL is added to diesel oil to form a kind of biodiesel fuel, which has high lubricity, flash point stability, low sulfur content, and suitable viscosity, and can be used in conventional diesel engine [20]. These promising market potentials urge the development of technologies on improving the efficiencies of producing EL, especially through cost-effective and environmentally friendly methods. To date, several researchers have reported the conversion of sucrose, cellulose, and biomass wastes into LE using inorganic liquid acids (especially sulfuric acid) as catalyst. For instance, Mascal et al. [21] commented on the processes for one-pot conversion of cellulose into EL, and the EL yield is on the order of 20%. Mao et al. [22] reported one pot two-step synthesis process for producing EL from paper pulp over H_2SO_4, and the EL yield reached 25.9 wt.%. Although these reactions were effective, the inorganic liquid acids have serious drawbacks in the aspects of separation and recycling, as well as equipment corrosion [23]. So, it is extremely important and necessary to develop new and environmentally benign catalysts with high activity

* Correspondence: zhaow1965@163.com

for the production of EL. In recent decades, solid acid catalyst as a heterogeneous catalyst has attracted extensive interest. It can overcome the above disadvantages of the inorganic acid in acid catalysis and has been widely applied to catalyze dehydration, alkylation, cracking, isomerization, esterification, acylation, and so on [24–27]. Among various solid acid catalysts, sulfated metal oxides have been widely concerned by researchers because of their strong acidity and excellent thermal stability. Therefore, sulfated metal oxides are expected to show high catalytic activity for the conversion of biomass to LE. For example, Sun et al. [28] applied a solid acid catalyst, USY, to convert cellulose to EL under anhydrous conditions, and the yield of ethyl levulinate reached 14.95%, whilst Li et al. [29] converted cellulose to EL over the composite solid acid $S_2O_8^{2-}/ZrO_2$/USY and the yield of EL reached 34.6%. Chang et al. [30] used SO_4^{2-}/ZrO_2/USY to catalyze the alcoholysis of cellulose to prepare EL, and the yield of EL was also significantly improved. In the early days, the researchers found that $Zr(SO_4)_2 \cdot 4H_2O$ has a highly acidity and a layered structure [31]. Zr^{4+} is in a state of severe electron deficiency and forms a strong coordination bond with oxygen atoms in bound water. On the other hand, oxygen atoms in sulfate radical form hydrogen bonds with bound water. Under the influence of these two aspects, the hydrogen in the water is severely delocalized, thus forming a Brønsted acid center [32,33]. Since $Zr(SO_4)_2$ has a small specific surface area, it is supported on a carrier with a high specific surface and dispersed on the carrier to expose acid active sites [34]. Mesoporous SiO_2 is a carrier with high specific surface area and loading $Zr(SO_4)_2$ onto the carrier will maximize its catalytic activity [35–37].

In this work, the highly acidic $Zr(SO_4)_2$ was loaded on mesoporous SiO_2 with high specific surface area (SSA) to prepare $Zr(SO_4)_2/SiO_2$ catalysts, which could solve the drawbacks of inorganic acid catalysts, improve the acidity of the catalysts, and then increase the catalytic activity. Then, wheat stalk powder (WSP) with complex structure was used as the raw material to produce EL over $Zr(SO_4)_2/SiO_2$ catalyst in an ethanol-cyclohexane system. The liquid product obtained from depolymerization of WSP was effectively separated by rotary evaporation. These results will be helpful to get insight into the conversion process of biomass to EL, and produce EL from wheat stalk by one-pot.

2. Materials and methods

2.1. Materials

Wheat stalk was collected from Xuzhou, Jiangsu, China. They were washed with water and then dried in sunlight, chopped into small pieces, and pulverized to pass through an 80-mesh sieve (<180 μm) to obtain wheat stalk powder (WSP). Tetraethyl orthosilicate (TEOS, 99%), ammonia solution, cetyltrimethylammonium bromide (CTAB, 99%), ethyl alcohol, and zirconium sulfatetetrahydrate were purchased from Sinopharm Chemical Reagent Co., Ltd. Cyclohexane was purchased from Aladdin Reagent Co., Ltd.

2.2. Preparation and characterization of catalyst

Mesoporous silica was prepared based on the method found in the literature [38]. Typically, CTAB (1 g) was completely dissolved in aqueous ammonia (1.2 mol/L, 110 mL) by ultrasonic vibration. Then, TEOS (5 mL) was added into the above solution. After stirring for 24 h at room temperature, the mixture was filtered and washed with deionized water to obtain a white solid, which was immersed in deionized water (400 mL) for 24 h. Then it was filtered and dried at 80 °C for 6 h. Finally, the mesoporous silica was obtained through calcining at 500 °C for 6 h, and subsequently employed as a support for the preparation of the solid acid catalyst.

$Zr(SO_4)_2/SiO_2$ solid acid catalyst was synthesized by the Stöber process [39]. A certain amount of $Zr(SO_4)_2$ was dissolved in deionized water (15 mL) by ultrasonic vibration, followed by adding the support SiO_2 (0.4 g) under magnetic stirring and being immersed at room temperature for 24 h. Then the water was evaporated and the left mixture was dried in a vacuum oven at 80 °C for 6 h to obtain $Zr(SO_4)_2/SiO_2$ solid acid catalyst.

The Fourier transform infrared (FTIR) spectra of the catalysts were recorded on a Nicolet Magna IR-560 FTIR spectrometer from 400 to 4000 cm^{-1}. Scanning electron microscopy (SEM) investigations were made using Quanta 200 (FEI, USA). Transmission electron microscopy (TEM) images were obtained from Tecnai-G2-F20 TEM (FEI, USA) with 0.14 nm of resolution combined with an energy dispersive spectrometer. X-ray diffraction (XRD) patterns were recorded with a Bruker D8 ADVNCE X-ray diffractometer (Bruker, Germany). The X-ray tube uses Cu as target and released Kα radiation when accelerated at 30 mA and 40 kV. The scanning rate and 2θ scanning angle range are 0.19451° per s and 3° to 90°, respectively. SSA, total pore volume (TPV) and average pore diameter (APD) of the catalysts were measured by nitrogen physical adsorption, using an autosorb-1 (Quantachrome, USA) at –196 °C. Before the tests, each sample was evacuated at 120 °C for 10 h.

Temperature-programed desorption of ammonia (NH_3-TPD), which was used to determine acid strength of catalysts, was carried out by a Quantachrome automated chemisorption flow analyzer with a TCD detector. Before each test, 30 mg sample was placed in a U-type quartz tube, flushed by helium flow at 120 °C for 60 min and cooled to 50 °C. After the

saturated adsorption of NH_3 on the catalyst surface, the sample was kept at 50 °C in helium flow for 60 min to remove physically adsorbed NH_3. The desorption of NH_3 was carried out from 50 °C to 600 °C at a heating rate of 15 °C·min^{-1}.

2.3. Preparation of EL from WSP

WSP (2.5 g), anhydrous ethanol (34 mL), cyclohexane (17 mL) and a certain amount of catalyst $Zr(SO_4)_2/SiO_2$ were added into a 200 mL stainless steel autoclave. After purging the air out of the autoclave with a vacuum pump at room temperature, the autoclave was heated to a certain temperature (160–220 °C) within 15 min and kept at that temperature for 30–70 min (reaction pressure varies with reaction temperature and the amounts of WSP and solvents). After the reaction was completed, the mixture was taken out from the autoclave and filtrated through a 0.8 μm membrane to obtain EL solution. Each experiment under the same conditions was repeated at least 3 times and the errors of the yields of EL based on WSP and the residue yields are within ±1%.

2.4. Separation of EL.

A three-step distillation method was used to separate EL from the obtained EL solution. The detailed process was shown in Figure 1. Firstly, the sample was distilled at 85 °C under normal pressure and the remainder was recorded as F_0. Then, sample F_0 was distilled under reduced pressure during 85–120 °C and the remainder was recorded as F_1. Sample F_1 was then treated by vacuum distillation between 120 °C and 150 °C. The last residue is light yellow liquid and is denoted as F_2. The composition of sample F_2 was analyzed with a Hewlett-Packard 6890/5973 gas chromatography-mass spectrometry (GC-MS) and an Agilent 1260 high performance liquid chromatogram (HPLC).

2.5. Analysis and calculation methods.

The concentrations of EL in the filtrate were determined by HPLC, equipped with a ZORBAX Eclipse Plus C_{18} column (4.6 × 250 mm, 5 m) and a diode array detector. The wavelength of chromatograph was set at 268 nm. In isocratic elution mode, a mixture of methanol and water (1:1 volume) was used as the mobile phase at a flow-rate of 1 mL.min^{-1}. The concentration of EL (C_{EL}) was determined via the external standard method, and the yield of EL based on WSP (Y_{EL}) was calculated according to the following formulae:

Y_{EL} (%) = $C_{EL}V/1000M_1 \times 100\%$ (based on WPS).

Where, C_{EL} is concentration of EL (mg mL^{-1}), V is volume of the filtrate (mL), M_1 is mass of WSP (g).

The residue yield (Y_R, %) was calculated as the mass ratio of residue (M_3–M_2, M_3, and M_2 denote the mass of filter cake and catalyst, respectively) and WSP (M_1) on dry basis, i.e., $Y_R = (M_3–M_2)/M_1 \times 100$.

Y_{EL}' and Y_R' denote EL yield and residue yield when no catalyst is used.

2.6. Influence transport phenomena on the catalysts

Investigation of transport influence in heterogeneous catalysis is of vital importance especially in a system that involves transfer of bulky molecules. This is investigated by using turnover frequency (TOF) value to comparatively check the activity of the catalyst. TOF is defined as the moles reacted per s per surface mole of the active species [40]. It quantifies the activity of the active center for catalytic reaction under a specific reaction condition by the number of molecules converted per unit time [41].

$$TOF = \frac{m_{EL}}{t \times f_m \times M_2}$$

Where m_{EL} is the amount in moles of EL (mmol); t is the reaction time (min); f_m is the amount of acid sites on the surface (mmol×g^{-1}).

3. Results and discussion

3.1. Characterization of catalyst $Zr(SO_4)_2/SiO_2$

FTIR spectra of the support and catalysts are shown in Figure 2. The infrared adsorption bands at 3448 cm^{-1} and 1631 cm^{-1} are attributed to the stretching frequency of physical adsorbed water [42], indicating that the sample contains a small amount of water. The peaks at 1088, 957, 794, and 461 cm^{-1} are assigned to the asymmetric stretching vibration of Si-O-Si, the stretching vibration of Si-OH, the symmetric stretching vibration of Si-O-Si and the bending vibration of Si-O-Si, respectively [43], indicating that the support may be SiO_2. In addition, no absorption peak of methylene was

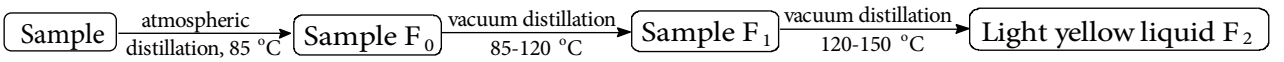

Figure 1. Flowchart of EL separation.

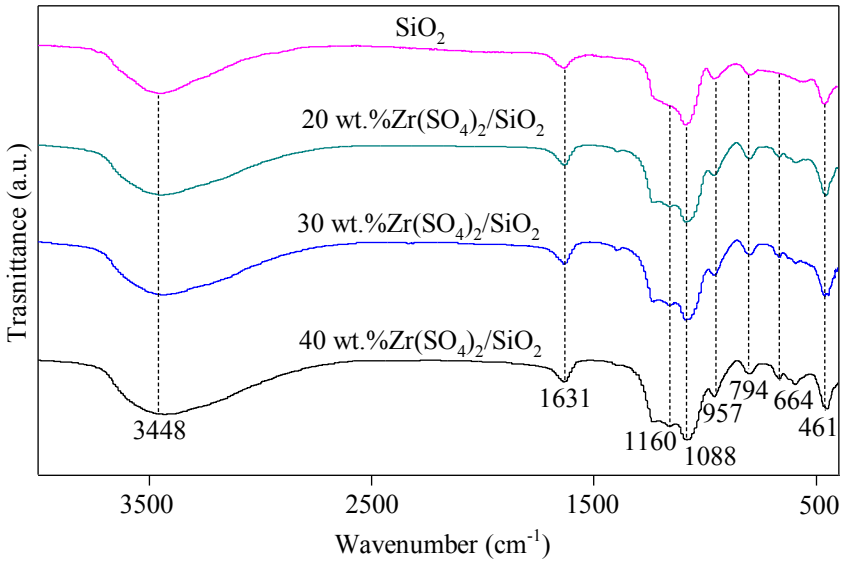

Figure 2. FTIR spectra of support and catalysts with different $Zr(SO_4)_2$ loadings.

detected in the support, indicating that CTAB was completely removed. The catalysts with different loadings of $Zr(SO_4)_2$ still have characteristic peaks of SiO_2, indicating that SiO_2 still exists on the catalysts. In addition, the FTIR spectra of catalysts with different $Zr(SO_4)_2$ loadings show the absorption peaks at 1160 and 664 cm^{-1}, and the intensity of these peaks increases with the increasing of $Zr(SO_4)_2$ loading. The adsorption band at 1160 cm^{-1} is characteristic of the asymmetric stretching vibration of S=O and the peak at 664 cm^{-1} was attributed to the asymmetric flexural vibration of O=S=O [44]. The existence of these peaks proves that the active component $Zr(SO_4)_2$ is loaded on the support.

From Figures 3a and 3b, a honeycomb-like pore structure can be observed in the TEM image of the support, because that CTAB forms a one-dimensional hexagonal ordered structure under alkaline condition [45,46]. The support SiO_2 was prepared through the aggregation of CTAB as structure-directing agent on the surface of the silica core under basic conditions, followed by subsequent hydrolysis and condensation of the TEOS as silica source [47]. When CTAB is decomposed during calcination, this regular pore structure can be formed. After $Zr(SO_4)_2$ (30 wt.%) is loaded, this pore structure becomes somewhat ambiguous as shown in Figures 3c and 3d. The possible reason is that the active component $Zr(SO_4)_2$ is filled into the pores of the support.

From EDS of the catalyst and support in Figure SI1 (left), the atom ratio (at, %) of Si and O is 1:2 in the support (as shown in Table 1). Furthermore, there are no other elements showed. During the test of TEM-EDS, C is caused by the carbon film as the bottom plate, while Cu is caused by the support of the copper mesh. All of these indicate that the prepared support is SiO_2. Besides Si and O elements, Zr and S elements are also detected in the catalyst, indicating that the active component is loaded on the support. As shown in Table 1 and Table 2, the atomic percentage of O element increases from 66.60% to 67.36%, which also proves that the active component is loaded on the support.

As shown in Figure 4, there are no obvious characteristic diffraction peaks of SiO_2 in XRD pattern of the support, indicating that the support SiO_2 is amorphous. The strong diffraction peaks at 13.50, 18.01, 20.54, 25.60, 29.60, 29.00, 30.70, 38.60, 42.30, and 45.80° are the characteristic peaks of $Zr(SO_4)_2$ [48]. The characteristic peaks of $Zr(SO_4)_2$ don't appear in the XRD patterns of catalysts with 30 wt.% and 40 wt.% $Zr(SO_4)_2$ loadings, but FTIR and TEM-EDS analysis show that the active component $Zr(SO_4)_2$ is loaded on the support, indicating that the active component $Zr(SO_4)_2$ is greatly dispersed on the support, which will also facilitate subsequent reactions.

The N_2 adsorption-desorption isotherms and pore size distribution of the prepared support and catalyst (30 wt.% $Zr(SO_4)_2/SiO_2$) are depicted in Figure 5. As shown in Figure 5a, the N_2 adsorption-desorption isotherms of support and catalyst are conventional IV type, and a typical H3 hysteresis loop appears in each curve, which proves that the sample contains a large number of micropores and mesopores [49]. From Figure 5b, the peak of the support at 2 nm is stronger, and there is also a weaker peak at less than 2 nm, indicating that the support is a mesoporous material with partial microporous. In the pore size distribution diagram of the catalyst, the peak shape and location of the catalyst are similar to those of the support, indicating that the loading process does not damage pore structure of the support. As listed in Table 3, the SSA falls down from 1166.11 in the support to 585.77 m^2g^{-1} in the catalyst after loading $Zr(SO_4)_2$ (30 wt.%), TPV

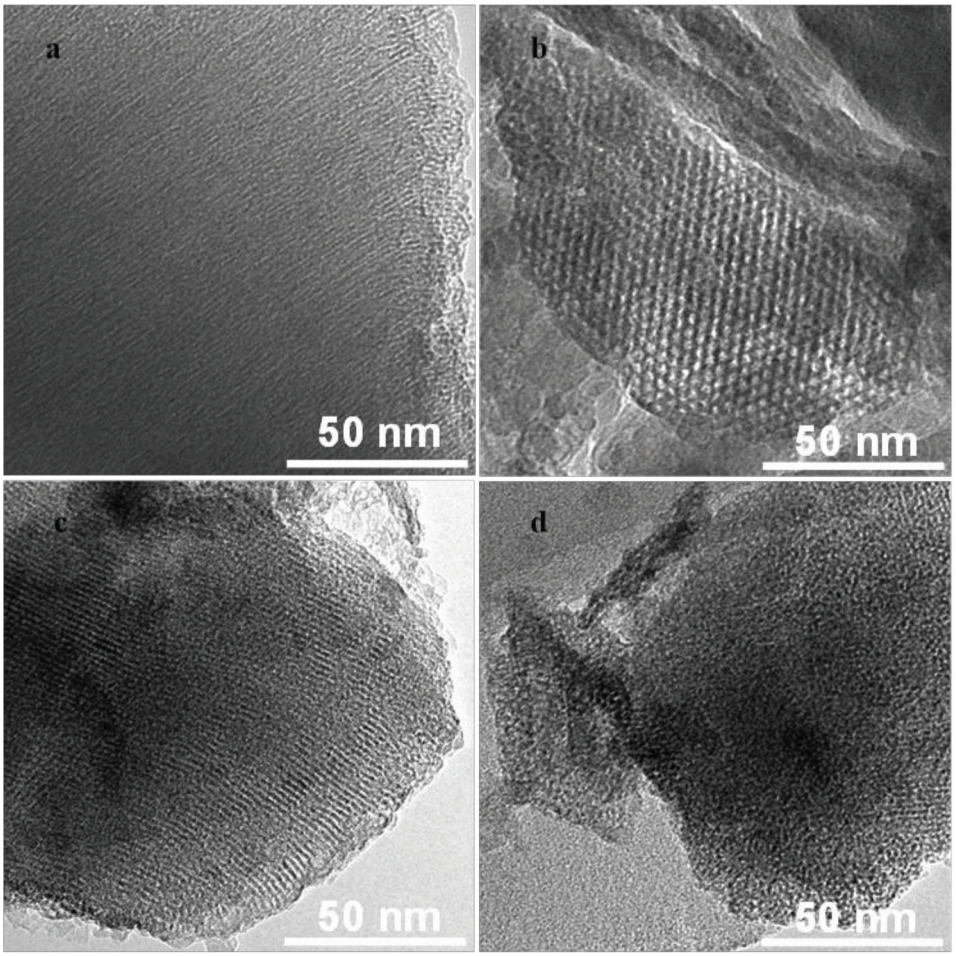

Figure 3. TEM images of samples: (a) SiO_2in top view; (b) SiO_2 in side view; (c) $Zr(SO_4)_2/SiO_2$ (30 wt.%) in top view; (d) and $Zr(SO_4)_2/SiO_2$ (30 wt.%) in side view.

Table 1. Relative element content of support.

Element	Wt (%)	At (%)
Si	46.70	33.30
O	53.30	66.60

Table 2. Relative element content of $Zr(SO_4)_2/SiO_2$ (30 wt.%).

Element	Wt (%)	At (%)
Si	38.82	28.92
O	51.67	67.36
S	3.65	2.38
Zr	5.85	1.34

decreases from 0.783 to 0.433 cm^3g^{-1}, and APD increases from 2.679 to 2.985 nm. All of these may be attributed to the load of $Zr(SO_4)_2$ on the carrier. The load of $Zr(SO_4)_2$ blocked a small fraction of the pores, which leaded to the decreasing of SSA and TPV. Furthermore, part of the pores was corroded due to the strong acidity of $Zr(SO_4)_2$, which also caused

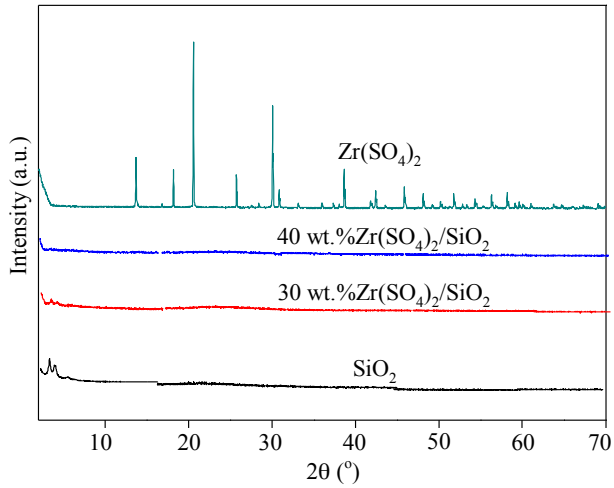

Figure 4. XRD patterns of SiO_2 and $Zr(SO_4)_2/SiO_2$ with different $Zr(SO_4)_2$ loadings.

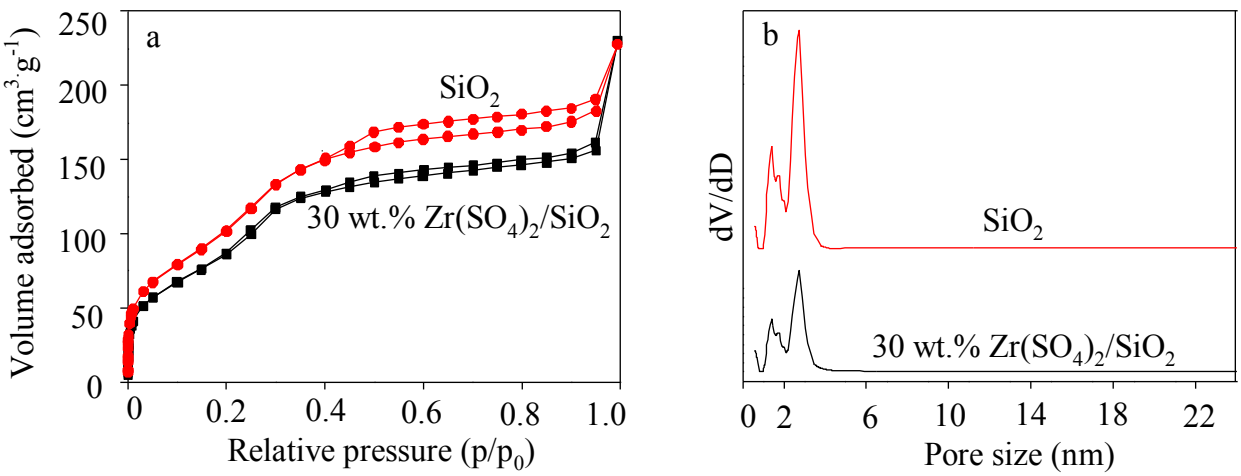

Figure 5. N_2 adsorption/desorption isotherms (a) and pore size distribution (b) of support and catalyst (30 wt.% $Zr(SO_4)_2/SiO_2$).

Table 3. Surface properties of SiO_2 and $Zr(SO_4)_2/SiO_2$ (30 wt.%).

Sample	SSA ($m^2 \cdot g^{-1}$)a	TPV($cm^3 \cdot g^{-1}$)b	APD (nm)[b]
SiO_2	1166.11	0.783	2.687
$Zr(SO_4)_2/SiO_2$	585.77	0.433	2.954

[a] SSA was calculated using the Brunauer–Emmett–Teller equation.
[b] TPV and average pore diameter were estimated using the Barret–Joyner–Halenda model.

the increasing of APD. Table SI1 presents the results of the surface area and porosity analysis of the catalysts with various $Zr(SO_4)_2/SiO_2$ loading except 30 wt.% $Zr(SO_4)_2/SiO_2$. The result showed that SSA decreased gradually from 1166.11 to 479.73 $m^2 \cdot g^{-1}$ with increasing $Zr(SO_4)_2$ loading, which was is because of the load of $Zr(SO_4)_2$ on the carrier.

The acidity of the catalysts was measured by NH_3-TPD analysis and the results are presented in Table 4. The results show that the total acidity is proportional to $Zr(SO_4)_2$ loading. The acidity of the support SiO_2 and catalysts with different $Zr(SO_4)_2$ loading was studied by NH_3-TPD, and the results were shown in Figure 6. The desorption peak of the support

Table 4. Catalytic performance of various catalysts for the conversions of WSP to EL.

Catalysts	Amount of acid sites (mmol×g^{-1})	Reaction conditions			Y_{EL} (%)	TOF (s^{-1})
		Temperature (°C)	Time (min)	Catalyst dosage (wt.%)		
10 wt.% $Zr(SO_4)_2/SiO_2$	3.187	190	50	24	10.90	3.3×10^{-4}
20 wt.% $Zr(SO_4)_2/SiO_2$	4.286	190	40	20	16.37	5.5×10^{-4}
30 wt.% $Zr(SO_4)_2/SiO_2$	5.264	190	50	20	17.14	3.8×10^{-4}
40 wt.% $Zr(SO_4)_2/SiO_2$	5.487	190	50	24	15.03	2.6×10^{-4}
1st-30 wt.% $Zr(SO_4)_2/SiO_2$	4.052	190	50	20	15.59	4.5×10^{-4}
2nd-30 wt.% $Zr(SO_4)_2/SiO_2$	3.194	190	50	20	10.32	3.7×10^{-4}
3rd-30 wt.% $Zr(SO_4)_2/SiO_2$	3.012	190	50	20	9.21	3.5×10^{-4}

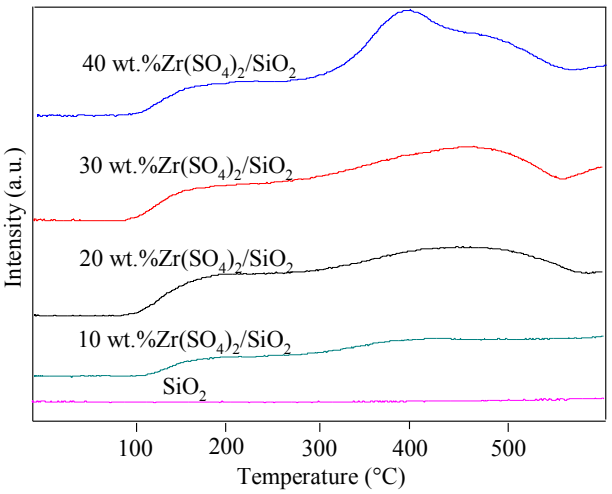

Figure 6. NH_3-TPD profiles of support and catalysts with different $Zr(SO_4)_2$ loading.

SiO_2 doesn't appear, indicating that the prepared SiO_2 is not acidic. The NH_3-TPD profiles of the catalysts show desorption peaks at around 200 °C and 400 °C, and the peak area increases with the increase of $Zr(SO_4)_2$ loading, demonstrating that the acid amount increases with the increasing of $Zr(SO_4)_2$ loading. It is generally believed that desorption peaks during 150–200 °C originate from weak acid site, and the peaks above 400 °C come from strong acid sites. The prepared catalysts have both weak acid sites and strong acid sites. On the one hand, Zr^{4+} with a severe electron deficient state forms a strong coordinate bond with the oxygen atom in the combined water. On the other hand, the oxygen atom in the sulfate has a hydrogen bond with the bound water. Under the action of these two aspects, the hydrogen in the water was severely delocalized, thereby forming a strong Brønsted acid center.

3.2. Preparation of EL from WSP over $Zr(SO_4)_2/SiO_2$

The effects of temperature, time, catalyst dosage and $Zr(SO_4)_2$ loading on Y_{EL} and Y_R are shown in Figure 7. From Figure 7a, Y_{EL} increased firstly and then decreased at the temperature range of 180 to 220 °C, and reached the maximum of 14.01% at 200 °C. At this temperature, Y_{EL}' was 2.29%. The appropriate temperature helps break glycosidic bond in the cellulose to form intermediate products, which are subsequently converted to EL. However, when the reaction temperature exceeded 200 °C, the intermediate 5-ethoxymethyl furfural (5-EMF) decomposed easily, resulting in the decreasing of Y_{EL}. During the whole reaction process, Y_R decreased firstly and then increased. In Figure 7b, Y_{EL} raised during 30 to 60 min and had a maximum yield of 14.75% at 60 min, while Y_{EL}' was 2.91%. But the Y_{EL} decreased when the reaction time exceeded 60 min, which may be related to the polymerization of the intermediates. As Figure 7c exhibits, with the increase of catalyst dosage from 16 wt.% (16 wt.% of WSP) to 24 wt.%, Y_{EL} increased to the maximum of 14.01%, while Y_{EL} decrease with the

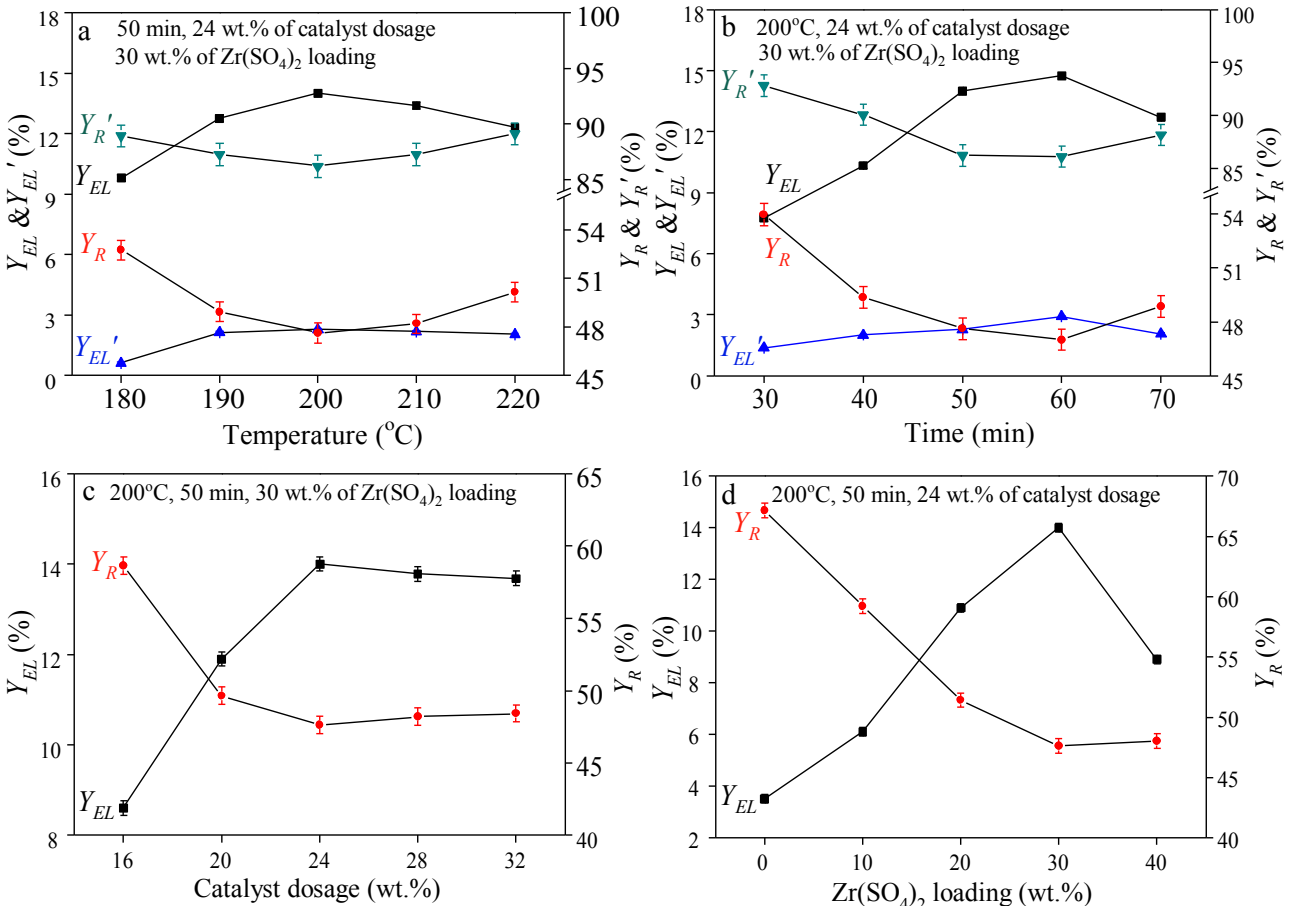

Figure 7. Effect of temperature, time, catalyst dosage, and $Zr(SO_4)_2$ loading on Y_{EL} and Y_R.

Table 5. Orthogonal test conditions and results [a].

Run	Temperature (°C)	Time (min)	Catalyst dosage (wt.%)	$Zr(SO_4)_2$ loading (wt.%)	Y_{EL} (%)
1	190	40	20	20	16.37
2	200	40	24	30	14.21
3	210	40	28	40	9.84
4	190	50	24	40	15.03
5	200	50	28	20	15.68
6	210	50	20	30	12.78
7	190	60	28	30	15.02
8	200	60	20	40	11.94
9	210	60	24	20	8.71
K_1	46.42	40.42	41.09	40.76	
K_2	41.83	43.49	37.95	42.01	
K_3	31.33	35.67	40.54	36.81	
R	15.09	7.82	3.14	5.20	

[a] K_i = summation of the test value of the same level, and $R = (1/3K_i)_{max} - (1/3K_i)_{min}$.

increasing of catalyst dosage from 24 wt.% to 32 wt.%. Figure 7d depicts the effect of $Zr(SO_4)_2$ loading on product yield. When $Zr(SO_4)_2$ loading increased from 0 to 30 wt.%, it was observed that Y_{EL} increased sharply from 3.53% to 14.01%, and reached the maximum of 14.01% under 30 wt.% of $Zr(SO_4)_2$ loading. More loading of $Zr(SO_4)_2$ can increase the number of acid sites, which promotes the formation of EL. However, when the loading of $Zr(SO_4)_2$ exceeds a certain value, too much acid sites can lead to an increase of side reactions, which hinders further increase of Y_{EL}.

The factors affecting Y_{EL} include reaction temperature, reaction time, catalyst dosage, and $Zr(SO_4)_2$ loading. A three-level-and-four-factor orthogonal test listed in Table 5 was designed to optimize the conditions. As a result, Y_{EL} reaches 17.14% under optimum conditions (i.e. 190 °C, 50 min, 20 wt.% of catalyst dosage and 30 wt.% of $Zr(SO_4)_2$ loading). Among them, the effect of reaction temperature on Y_{EL} is the most notable. This Y_{EL} has almost unchanged compared with Y_{EL} (17.91%) obtained by Chang et al. [50] using H_2SO_4 to catalyze wheat stalk under optimum conditions. However, our study has solved the problems that the inorganic liquid acids have serious drawbacks in the aspects of separation and recycling, as well as equipment corrosion, which makes the catalyst $Zr(SO_4)_2/SiO_2$ a good process practicability. Moreover, WSP reaches a high conversion rate ($1-Y_R$, %) under this condition, which provides a reference for the related work of catalytic conversion of wheat stalk.

Table 4 shows the activity of various catalysts for the conversions of WSP to EL based on TOF and Y_{EL}. It is obvious that 20 wt.% $Zr(SO_4)_2/SiO_2$ shows the maximal TOF of 5.5×10^{-4} s^{-1} when reaction temperature, time, and catalyst dosage are 190 °C, 40 min, and 20 wt.%, respectively. However, 30 wt.% $Zr(SO_4)_2/SiO_2$ presents the maximal Y_{EL} of 17.14% when reaction temperature, time, and catalyst dosage are 190 °C, 50 min, and 20 wt.%, respectively. Since TOF evaluates the catalyst activity by the amount of products generated at the unit acid site in the catalyst per unit time, the results of the catalyst activity based on TOF and Y_{EL} evaluation are small different.

3.3. Reaction kinetics of producing EL from WSP over $Zr(SO_4)_2/SiO_2$

The reaction kinetics of producing EL from WSP over $Zr(SO_4)_2/SiO_2$ was investigated by examining the relationship between WSP conversion (x, %) at 190 °C and reaction time. As Figure 8 shows, neglecting the impact of temperatures and catalyst deactivation on the reaction order, good linear relations between $\ln(1-x)^{-1}$ and the reaction time t suggest that the reaction of producing EL from WSP over $Zr(SO_4)_2/SiO_2$ is a close first-order. The relation between x and t can be expressed as: $t = k^{-1}\ln(1-x)^{-1}$, where k and x are denoted as the rate constant and WSP conversion, respectively. Calculated from the slopes of $\ln(1-x)^{-1}$ versus t, rate constants were 0.075 h^{-1} and 0.019 h^{-1} when $Zr(SO_4)_2/SiO_2$ was used as the catalyst and without catalyst, indicating that the catalyst $Zr(SO_4)_2/SiO_2$ has better catalytic performance for the conversion of WSP to EL.

The total ion chromatogram (TIC) of sample F_2 from the separation and purification of EL solution is shown in Figure 9. The result verifies that the main component of sample F_2 is EL and its relative content is up to 91.73%. Further, HPLC was used to detect the composition of sample F_2. As shown in Figure SI2, the relative content of EL reaches 90.35%, indicating that the separation method is effective.

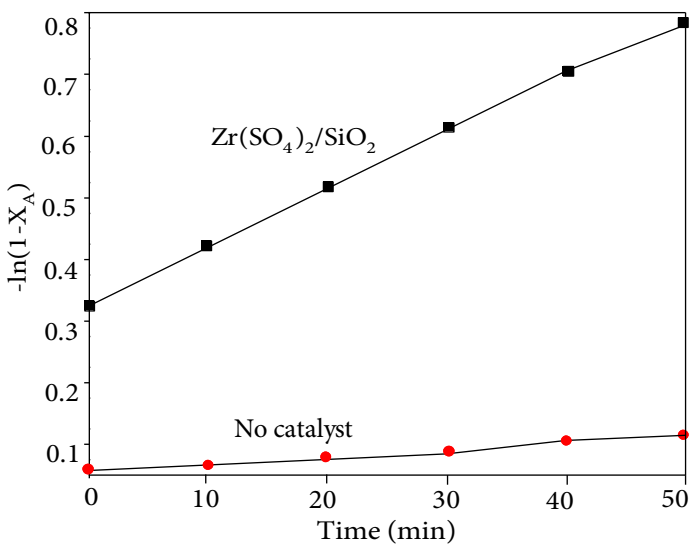

Figure 8. Kinetic curves of producing EL from WSP over $Zr(SO_4)_2/SiO_2$ and no catalyst.

3.4. Reaction pathway

Combined with the experimental results and references [51,52], the reaction pathway was speculated and shown in Figure 10. Under the attack of H^+ from the catalyst, the glycosidic bond of cellulose in WSP breaks to afford glucose, and the conversion of glucose to EL may be through two ways. The first way is that glucose reacts with ethanol under the action of H^+, and one molecule of water is removed to form ethyl glucoside. Ethyl glucoside is dehydrated under acidic condition to produce 5-EMF, and 5-EMF reacts with one molecule of water and one molecule of ethanol under acid conditions to afford EL. Another possible way is that glucose is firstly isomerized to fructose under acidic condition, and fructose is dehydrated under acidic condition to form 5-hydroxymethyl furfural (5-HMF). 5-HMF is hydrolyzed to form LA, and LA is esterified with ethanol to generate EL.

3.5. Catalyst reusability

Long-term stability of heterogeneous catalyst is an extremely important characteristic to reduce production cost in practical use. Reusability of 30 wt.% $Zr(SO_4)_2/SiO_2$ was studied to ascertain its durability and economic viability by the method of Peng et al. [53] with slight modifications for calcination conditions (400 °C, 1.5 h), and shown in Table 4. The catalysts were recovered by calcination to remove WSP. The recovered catalysts of 30 wt.% $Zr(SO_4)_2/SiO_2$ were denoted as 1st-30 wt.% $Zr(SO_4)_2/SiO_2$, 2nd-30 wt.% $Zr(SO_4)_2/SiO_2$, and 3rd-30 wt.% $Zr(SO_4)_2/SiO_2$. After three cycles, the recovery yield of 30 wt.% $Zr(SO_4)_2/SiO_2$ was about 92.26%, the acid sites number of 30 wt.% $Zr(SO_4)_2/SiO_2$ decreased from 5.264 mmol×g^{-1} to

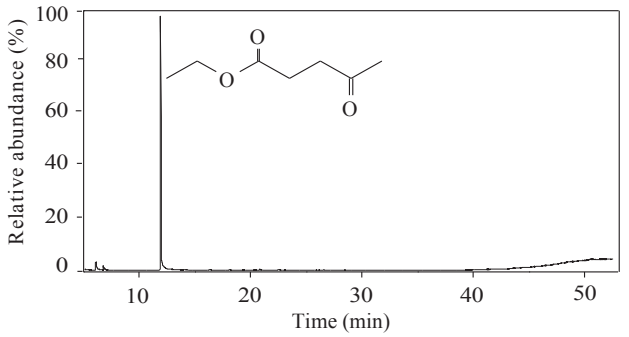

Figure 9. TIC of sample F_2.

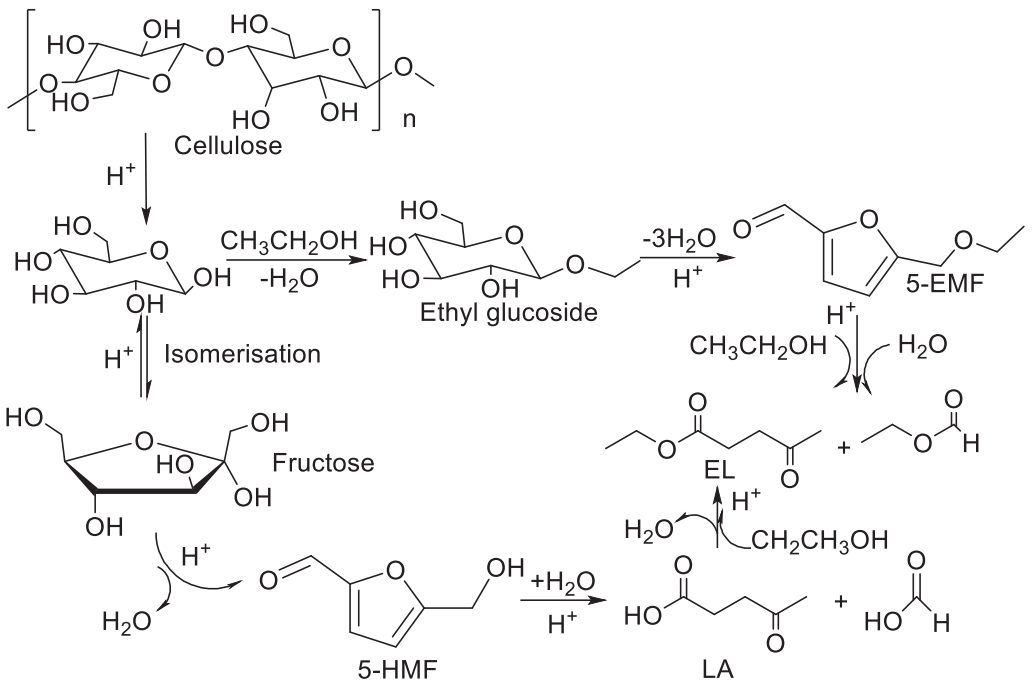

Figure 10. Reaction pathway in the production of EL.

3.012 mmol×g^{-1}, Y_{EL} was reduced from 17.14% to 9.21%, which may be attributed to the leaching of active phase $Zr(SO_4)_2/SiO_2$. From Figure SI3 and Table SI2, the relative content of sulfur dropped from 3.65 wt.% to 2.54 wt.% in the first run compared with the fresh 30 wt.% $Zr(SO_4)_2/SiO_2$ catalyst. In the subsequent two cycles, the thermally regenerated catalyst was maintained at about 1.40 wt.% of sulfur relative content. In summary, the SO_4^{2-} was partially leached from $Zr(SO_4)_2/SiO_2$ catalyst after the first operation. In the following two cycles, the thermally regenerated catalyst was found to remain active with almost unchanged Y_{EL} and relative element content, indicating a good stability.

4. Conclusion

$Zr(SO_4)_2/SiO_2$ was prepared by impregnating $Zr(SO_4)_2$ onto mesoporous silica. According to multiple characterizations, $Zr(SO_4)_2$ is successfully attached to the prepared support SiO_2 and the acidity increases with the increasing of $Zr(SO_4)_2$ loading. $Zr(SO_4)_2/SiO_2$ exhibits high catalytic activity for the conversion of WSP to EL. Based on catalytic performance and reaction kinetics of $Zr(SO_4)_2/SiO_2$ research, $Zr(SO_4)_2/SiO_2$ can effectively catalyze the conversion of WSP to EL. A comparative study showed that 20 wt.% $Zr(SO_4)_2/SiO_2$ exhibits higher catalytic activity than other catalysts with different $Zr(SO_4)_2$ loadings. Y_{EL} reaches maximum value of 17.14% when reaction temperature, reaction time, catalyst dosage, and $Zr(SO_4)_2$ loading are 190 °C, 50 min, 20 wt.% and 30 wt.%, respectively. The relative content of EL is more than 90% after three steps of distillation. This study provides an efficient way to prepare valuable chemical EL by catalytic conversion of WSP. Furthermore, high conversion of wheat stalk is obtained under this condition, which provides a reference for catalytic conversion and efficient utilization of wheat stalk.

Acknowledgment

This work was subsidized by the Fundamental Research Funds for the Central Universities (Grant 2017XKZD10).

References

1. Xu XL, Zhang XL, Zou WJ, Yue HJ, Tian G et al. Conversion of carbohydrates to methyl levulinate catalyzed by sulfated montmorillonite. Catalysis Communications 2015; 62: 67-70. doi: 10.1016/j.catcom.2015.01.011
2. Zhao SQ, Xu GZ, Chang C, Fang SQ, Liu Z et al. Direct conversion of carbohydrates into ethyl levulinate with potassium phosphotungstate as an efficient catalyst. Catalysts 2015; 5 (4): 1897-1910.doi: 10.3390/catal5041897
3. Saravanamurugan S, Riisager A. Zeolite catalyzed transformation of carbohydrates to alkyl levulinates. ChemCatChem 2013; 5 (7): 1754-1757. doi: 10.1002/cctc.201300006
4. Tan ZF, Chen KT, Liu PK, Possibilities and challenges of China's forestry biomass resource utilization. Renewable and Sustainable Energy Reviews 2015; 41: 368-378. doi: 10.1016/j.rser.2014.08.059
5. Climent MJ, Corma A, Iborra S. Conversion of biomass platform molecules into fuel additives and liquid hydrocarbon fuels. Green Chemistry 2014; 16 (2): 516-547. doi: 10.1039/C3GC41492B
6. Loow YL, Wu TY, Tan KA, Lim YS, Siow LF et al. Recent advances in the application of inorganic salt pretreatment for transforming lignocellulosic biomass into reducing sugars. Journal of Agricultural and Food Chemistry 2015; 63 (38): 8349-8363. doi: 10.1021/acs.jafc.5b01813
7. Tan TW, Shang F, Zhang X. Current development of biorefinery in China. Biotechnology Advances 2010; 28 (5): 543-555. doi: 10.1016/j.biotechadv.2010.05.004
8. Lal R. World crop residues production and implications of its use as a biofuel. Environment International 2005; 31 (4): 575-584. doi: 10.1016/j.envint.2004.09.005
9. Zeng XY, Ma YT, Ma LR. Utilization of straw in biomass energy in China. Renewable and Sustainable Energy Reviews 2007; 11 (5): 976-987. doi: 10.1016/j.rser.2005.10.003
10. Mood SH, Golfeshan AH, Tabatabaei M, Jouzani GS, Najafi G et al. Lignocellulosic biomass to bioethanol, a comprehensive review with a focus on pretreatment. Renewable and Sustainable Energy Reviews 2013; 27: 77-93. doi: 10.1016/j.rser.2013.06.033
11. Tadesse H, Luque R. Advances on biomass pretreatment using ionic liquids: an overview. Energy & Environmental Science 2011; 4 (10): 3913-3929. doi: 10.1039/C0EE00667J
12. Prasad S, Singh A, Joshi HC. Ethanol as an alternative fuel from agricultural, industrial and urban residues. Resources Conservation and Recycling 2007; 50 (1): 1-39. doi: 10.1016/j.resconrec.2006.05.007
13. Chang C, Xu GZ, Zhu WN, Bai J, Fang SQ. One-pot production of a liquid biofuel candidate—ethyl levulinate from glucose and furfural residues using a combination of extremely low sulfuric acid and zeolite USY. Fuel 2015; 140: 365-370. doi: 10.1016/j.fuel.2014.09.102

14. Zhang XY, Li Y, Xue LF, Wang ST, Wang XH et al. Catalyzing cascade production of methyl levulinate from polysaccharides using heteropoly acids $H_nPW_{11}MO_{39}$ with Brønsted/Lewis acidic sites. ACS Sustainable Chemistry & Engineering 2018; 6 (1): 165-176. doi: 10.1021/acssuschemeng.7b02042

15. Morales G, Osatiashtiani A, Hernandez B, Iglesias J, Melero JA et al. Conformal sulfated zirconia monolayer catalysts for the one-pot synthesis of ethyl levulinate from glucose. Chemical Communications 2014; 50 (79): 11742-11745. doi: 10.1039/C4CC04594G

16. Demolis A, Essayem N, Rataboul F. Synthesis and applications of alkyl levulinates. ACS Sustainable Chemistry & Engineering 2014; 2 (6): 1338-1352. doi: 10.1021/sc500082n

17. Khusnutdinov RI, Baiguzina AR, Smirnov AA, Mukminov RR, Whemilev UM. Furfuryl alcohol in synthesis of levulinic acid esters and difurylmethane with Fe and Rh complexes. Russian Journal of Applied Chemistry 2007; 80 (10): 1687-1690. doi: 10.1134/S1070427207100163

18. Joshi H, Moser BR, Toler J, Smith WF, Walker T. Ethyl levulinate: a potential bio-based diluent for biodiesel which improves cold flow properties. Biomass & Bioenergy 2011; 35 (7): 3262-3266. doi: 10.1016/j.biombioe.2011.04.020

19. Windom BC, Lovestead TM, Mascal M, Nikitin EB, Bruno TJ. Advanced distillation curve analysis on ethyl levulinate as a diesel fuel oxygenate and a hybrid biodiesel fuel. Energy & Fuels 2011; 25 (4): 1878-1890. doi: 10.1021/ef200239x

20. Fiorentino G, Ripa M, Mellino S, Fahd S, Ulgiati S. Life cycle assessment of Brassica carinata biomass conversion to bioenergy and platform chemicals. Journal of Cleaner Production 2014; 66: 174-187. doi: 10.1016/j.jclepro.2013.11.043

21. Mascal M, Nikitin EB. Comment on processes for the direct conversion of cellulose or cellulosic biomass into levulinate esters. ChemSusChem 2010; 3: 1349-1351. doi:10.1002/cssc.201000326

22. Mao RLV, Zhao Q, Dima G, Petraccone D. New process for the acid-catalyzed conversion of cellulosic biomass (AC3B) into alkyl levulinates and other esters using a unique one-pot system of reaction and product extraction. Catalysis Letters 2011; 141 (2): 271-276. doi: 10.1007/s10562-010-0493-y

23. Lange JP, Van de Graaf WD, Haan RJ. Conversion of furfuryl alcohol into ethyl levulinate using solid acid catalysts. ChemSusChem 2009; 2 (5): 437-441. doi: 10.1002/cssc.200800216

24. Moradi GR, Yaripour F, Vale-Sheyda P. Catalytic dehydration of methanol to dimethyl ether over mordenite catalysts. Fuel Processing Technology 2010; 91 (5): 461-468. doi: 10.1016/j.fuproc.2009.12.005

25. Busca G. Acid catalysts in industrial hydrocarbon chemistry. Chemical Reviews 2007; 107 (11): 5366-5410. doi: 10.1021/cr068042e

26. Tyagi B, Mishra MK, Jasra RV. Synthesis of 7-substituted 4-methyl coumarins by Pechmann reaction using nano-crystalline sulfated-zirconia. Journal of Molecular Catalysis A: Chemical 2007; 276 (1-2): 47-56. doi: 10.1016/j.molcata.2007.06.003

27. Yu GX, Zhou XL, Li CL, Chen LF, Wang JA. Esterification over rare earth oxide and alumina promoted SO_4^{2-}/ZrO_2. Catalysis Today 2009; 148 (1-2): 169-173. doi: 10.1016/j.cattod.2009.03.006

28. Sun PQ, Zhao SQ, Chang C, Chen JW. Study on production of ethyl levulinate from cellulose catalyzed by solid acid USY. Journal of Zhengzhou University (Engineering Science) 2014; 35 (3): 22-26. doi: 10.3969/j.issn.1671-6833.2014.03.006

29. Li B, Chang C, Zhu WN, Wang LF, Zhu F, Qiao JY. Experimental study on ethyl levulinate production from cellulose catalyzed by solid acid catalyst. Acta Energiae Solaris Sinica 2015; 36 (7): 1768-1772. doi: CNKI:SUN:TYLX.0.2015-07-037

30. Chang C, An R, Kong PF. Alcoholysis of cellulose into ethyllevulinate catalyzed by SO_4^{2-}/ZrO_2/USY. Journal of Zhengzhou University (Engineering Science) 2018; 39 (2): 80-85. doi: 10.13705/j.issn.1671-6833.2017.05.010

31. Juan JC, Zhang JC, Yarmo MA. Efficient esterification of fatty acids with alcohols catalyzed by $Zr(SO_4)_2{\cdot}4H_2O$ under solvent-free condition. Catalysis Letters 2008; 126 (3-4): 319-324. doi: 10.1007/s10562-008-9622-2

32. Juan JC, Zhang JC, Jiang YJ, Cao WL, Yarmo MA. The zirconium sulfate microcrystal structure in relation to their activity in the esterification. Journal of Molecular Catalysis A: Chemical 2007; 272 (1-2): 91-95. doi: 10.1016/j.molcata.2007.03.028

33. Figueras F. Pillared clays as catalysts. Catalysis Reviews Science and Engineering 1988; 30: 457-499. doi: 10.1080/01614948808080811

34. Liao YH, Liu QY, Wang TJ, Long JX, Zhang Q et al. Promoting hydrolytic hydrogenation of cellulose to sugar alcohols by mixed ball milling of cellulose and solid acid catalyst. Energy & Fuels 2014; 28 (9): 5778-5784. doi: 10.1021/ef500717p

35. Ren W, Liu CH, Lian S, Li ZP. Flow cytometry-assisted mix-and-read assay for ultrasensitive detection of protein kinase activity by use of Zr^{4+}-functionalized mesoporous SiO_2 microspheres. Analytical Chemistry 2013; 85 (22): 10956-10961. doi: 10.1021/ac4024457

36. Juan JC, Zhang JC. Structure and reactivity of silica-supported zirconium sulfate for esterification of fatty acid under solvent-free condition. Applied Catalysis A: General 2007; 332 (2): 209-215. doi: 10.1016/j.apcata.2007.08.016

37. Garcia-Sancho C, Cecilia JA, Merida-Robles JM, Gonzalez JS, Moreno-Tost R et al. Effect of the treatment with H_3PO_4 on the catalytic activity of Nb_2O_5 supported on Zr-doped mesoporous silica catalyst. Case study: glycerol dehydration. Applied Catalysis B: Environmental 2018; 221: 158-168. doi: 10.1016/j.apcatb.2017.09.016

38. Ruffino F, Tomasello MV, Miritello M, De Bastiani R, Nicotra G et al. Analyses of the As doping of SiO_2/Si/SiO_2 nanostructures. In: Kissinger G, Pizzini S, Tu H, Yamada Kaneta H (editors). Physica Status Solidi C: Current Topics in Solid State Physics. Weinheim, GER: Wiley, 2011, pp.863-866.

39. Guo YH, Wang YH, Hu CW, Wang YH, Wang EB et al. Microporous polyoxometalates POMs/SiO_2: synthesis and photocatalytic degradation of aqueous organocholorine pesticides. Chemistry of Materials 2000; 12 (11): 3501-3508. doi: 10.1021/cm000074+

40. Madon RJ, Boudart M. Experimental criterion for the absence of artifacts in the measurement of rates of heterogeneous catalytic reactions. Industrial and Engineering Chemistry Research Fundamentals 1902; 21: 438-447. doi: 10.1021/i100008a022

41. Boudart M. Turnover rates in heterogeneous catalysis. Chemical Reviews 1995; 95: 661-666. doi: 10.1021/cr00035a009

42. Braun JV, Santos SJ, Espindola GD, Fontoura LAM, Alves AK. Microwave heating and synthesis method influence in SiO_2-ZrO_2 mixed oxides preparation and its use as heterogeneous catalyst for biodiesel obtainment. Reaction Kinetics Mechanisms and Catalysis 2021; 132: 921-934. doi: 10.1007/s11144-021-01950-9

43. Ma YD, Wang YR, Wu WQ, Zhang JY, Cao YN et al. Slurry-phase hydrocracking of a decalin-phenanthrene mixture by MoS_2/SiO_2-ZrO_2 bifunctional catalysts. Industrial & Engineering Chemistry Research 2021; 60: 230-242. doi: 10.1021/acs.iecr.0c04999

44. Zhou HB, Gao Y, Li J. Research of preparation of SO_4^{2-}/$TiO^{2-}ZrO_2$ and its application on synthesis of biodiesel from waste cooking oil. Applied Mechanics and Materials 2013; 316-317: 906-910. doi: 10.4028/www.scientific.net/AMM.316-317.906

45. Gu YJ, Yan B. Europium (III) complex functionalized Si-MCM-41 hybrid materials with visible-light-excited luminescence. Inorganica Chimica Acta 2013; 408: 96-102. doi: 10.1016/j.ica.2013.09.008

46. Mendez FJ, Llanos A, Echeverria M, Jauregui R, Villasana Y et al. Mesoporous catalysts based on Keggin-type heteropoly acids supported on MCM-41 and their application in thiophene hydride sulfurization. Fuel 2013; 110: 249-258. doi: 10.1016/j.fuel.2012.11.021

47. Kim JH, Yoon SB, Kim JY, Chae YB, Yu JS. Synthesis of monodisperse silica spheres with solid core and mesoporous shell: morphological control of mesopores. Colloids and Surfaces A: Physicochemical and Engineering Aspects 2008; 313-314: 77-81. doi: 10.1016/j.colsurfa.2007.04.145

48. Juan JC, Zhang JC, Yarmo MA. Study of catalysts comprising zirconium sulfate supported on a mesoporous molecular sieve HMS for esterification of fatty acids under solvent-free condition. Applied Catalysis A: General 2008; 347 (2): 133-141. doi: 10.1016/j.apcata.2008.06.004

49. Evangelista JPC, Chellappa T, Coriolano ACF, Fernandes VJ, Souza LD et al. Synthesis of alumina impregnated with potassium iodide catalyst for biodiesel production from rice bran oil. Fuel Processing Technology 2012; 104: 90-95. doi: 10.1016/j.fuproc.2012.04.028

50. Chang C, Xu GZ, Jiang XX. Production of ethyl levulinate by direct conversion of wheat straw in ethanol media. Bioresource Technology 2012; 121: 93-99. doi: 10.1016/j.biortech.2012.06.105

51. Chang JL, Bai J, Chang C, Zhao SQ, Li HL et al. Products distribution of glucose through ethanolysis reaction catalyzed by extremely low acid under high temperature. Chemistry and Industry of Forest Products 2015; 35: 8-14. doi: 10.3969/j.issn.0253-2417.2015.06.002

52. Zu WN, Chang C, Ma C, Du FG. Kinetics of glucose ethanolysis is catalyzed by extremely low sulfuric acid in ethanol medium. Chinese Journal of Chemical Engineering 2014; 22 (2): 238-242. doi: 10.1016/S1004-9541(14)60049-5

53. Peng LC, Lin L, Zhang JH, Shi JB, Liu SJ. Solid acid catalyzed glucose conversion to ethyl levulinate. Applied Catalysis A: General 2011; 397 (1-2): 259-265. doi: 10.1016/j.apcata.2011.03.008